

THE BLENDING TOOLKIT:
A SIMULATION FRAMEWORK FOR EVALUATION OF GALAXY DETECTION AND DEBLENDING

ISMAEL MENDOZA^{1,*}, ANDRII TORCHYLO^{2,†}, THOMAS SAINRAT^{3,4,‡}, AXEL GUINOT^{4,5}, ALEXANDRE BOUCAUD⁴, MAXIME PAILLASSA⁶, CAMILLE AVESTRUZ^{1,7}, PRAKRUTH ADARI⁸, ERIC AUBOURG⁹, BISWAJIT BISWAS⁴, JAMES BUCHANAN¹⁰, PATRICIA BURCHAT¹¹, CYRILLE DOUX¹², REMY JOSEPH¹³, SOWMYA KAMATH², ALEX I. MALZ⁵, GRANT MERZ¹⁴, HIRONAO MIYATAKE^{15,16,17}, CÉCILE ROUCELLE⁴, TIANQING ZHANG^{5,18,19}, AND THE LSST DARK ENERGY SCIENCE COLLABORATION

¹Department of Physics, University of Michigan, Ann Arbor, MI 48105, USA

²Department of Physics, Stanford University, Stanford, CA 94305, USA

³Université de Strasbourg, CNRS, IPHC UMR 7178, F-67000 Strasbourg, France

⁴Université Paris Cité, CNRS, AstroParticule et Cosmologie, F-75013, Paris, France

⁵McWilliams Center for Cosmology, Department of Physics, Carnegie Mellon University, Pittsburgh, PA 15213, USA

⁶Department of Physics, Graduate School of Science, Nagoya University, Furo-cho Chikusa-ku, Nagoya 464-8602, Japan

⁷Leinweber Center for Theoretical Physics, University of Michigan, Ann Arbor, MI 48109, USA

⁸Department of Physics and Astronomy, Stony Brook University, Stony Brook, NY 11794-3800, USA

⁹Université Paris Cité, CNRS, CEA, AstroParticule et Cosmologie, F-75013, Paris, France

¹⁰Physics Division, Lawrence Livermore National Laboratory, Livermore, CA 94306, USA

¹¹Kavli Institute for Particle Astrophysics and Cosmology, Department of Physics, Stanford University, Stanford, CA 94305, USA

¹²Univ. Grenoble Alpes, CNRS, Grenoble INP, LPSC-IN2P3, 38000 Grenoble, France

¹³The Oskar Klein Centre, Department of Physics, Stockholm University, Albanova University Center, Stockholm, SE-10691, Sweden.

¹⁴Department of Astronomy, University of Illinois at Urbana-Champaign, 1002 West Green Street, Urbana, IL 61801, USA

¹⁵Kobayashi-Maskawa Institute for the Origin of Particles and the Universe (KMI), Nagoya University, Nagoya, 464-8602, Japan

¹⁶Institute for Advanced Research, Nagoya University, Nagoya, 464-8601, Japan

¹⁷Kavli Institute for the Physics and Mathematics of the Universe (WPI), The University of Tokyo Institutes for Advanced Study (UTIAS), The University of Tokyo, Chiba 277-8583, Japan

¹⁸Department of Physics and Astronomy and PITT PACC, University of Pittsburgh, Pittsburgh, PA 15260, USA and

¹⁹SLAC National Accelerator Laboratory, 2575 Sand Hill Road, Menlo Park, CA 94025, USA

Version September 30, 2024

ABSTRACT

We present an open source Python library for simulating overlapping (i.e., *blended*) images of galaxies and performing self-consistent comparisons of detection and deblending algorithms based on a suite of metrics. The package, named *Blending Toolkit* (BTK), serves as a modular, flexible, easy-to-install, and simple-to-use interface for exploring and analyzing systematic effects related to blended galaxies in cosmological surveys such as the Vera Rubin Observatory Legacy Survey of Space and Time (LSST). BTK has three main components: (1) a set of modules that perform fast image simulations of blended galaxies, using the open source image simulation package GALSIM; (2) a module that standardizes the inputs and outputs of existing deblending algorithms; (3) a library of deblending metrics commonly defined in the galaxy deblending literature. In combination, these modules allow researchers to explore the impacts of galaxy blending in cosmological surveys. Additionally, BTK provides researchers who are developing a new deblending algorithm a framework to evaluate algorithm performance and make principled comparisons with existing deblenders. BTK includes a suite of tutorials and comprehensive documentation. The source code is publicly available on GitHub at <https://github.com/LSSTDESC/BlendingToolKit>.

1. INTRODUCTION

Modern ground-based cosmological surveys, including the Dark Energy Survey (Dark Energy Survey Collaboration et al. 2016), the Hyper Suprime-Cam Subaru Strategic Program (Aihara et al. 2018), and the upcoming Rubin Observatory Legacy Survey of Space and Time (LSST, Ivezić et al. 2019)) will detect an unprecedented number of galaxies and have the potential to significantly improve our understanding of the

Universe. As the sensitivity of these surveys increases, so does the density of detectable light sources (stars and galaxies), which in turn increases the rate at which sources overlap with each other in images. This phenomenon, known as *blending*, is a major potential source of systematic bias and uncertainty for modern surveys (Melchior et al. 2021); blending undermines our ability to identify individual sources in a given image (Dawson et al. 2016; Troxel et al. 2023) and disentangle their properties, such as flux and shape, from those of neighboring sources (Dawson et al. 2016; Hoekstra et al. 2017; Euclid Collaboration et al. 2019).

In LSST, it is predicted that about 60% of galaxies will be blended to some degree (at full-depth, i.e. $r \simeq 27.2$) (Sanchez

* Corresponding Author: imendoza@umich.edu.

† Corresponding Author: torchylo@stanford.edu.

‡ Corresponding Author: thomas.sainrat@iphc.cnrs.fr.

★ These authors contributed equally.

For more details on author contributions, see Section 6.

et al. 2021), 51% of galaxies will be overlapping with sources that can be detected individually (at depth $r \simeq 24$) (Eckert et al. 2020), and that between 15% and 30% of galaxies in i -band images will be part of *unrecognized blends* (at depth $i \simeq 27$ and $i \simeq 26$ respectively) (Dawson et al. 2016; Troxel et al. 2023) – i.e., blends that are detected as a single object, but actually correspond to two or more sources. For HSC, it was estimated that about 58% of the detected objects in the i -band wide survey are blended sources (at depth $r \simeq 26$) (Bosch et al. 2017). Since a large fraction of the galaxies detected in modern surveys will be impacted by blending, blended objects cannot be discarded without losing a significant amount of statistical power (Chang et al. 2013, 2015) and inducing selection bias in the cosmological probes (Hartlap et al. 2011). Thus, we need an accurate understanding of the systematic errors that blending contributes to our measurements, and robust algorithms to mitigate these errors.

Blending impacts the two most important static probes of dark energy for ground-based cosmological surveys: weak gravitational lensing and galaxy clusters. Weak gravitational lensing uses the fact that observed galaxy shapes trace the underlying dark matter distribution (Huterer 2002; Kilbinger 2015). In principle, blending impacts the three types of two-point statistics (cosmic shear, galaxy-galaxy lensing, and galaxy clustering) commonly used in weak lensing analyses, although its effect on cosmic shear has been most widely studied. *Cosmic shear* is the relatively small, approximately linear distortion of shapes by weak lensing from large-scale mass distributions. Blending can introduce several types of potential bias in measured shear: selection bias due to detection inefficiency for blended galaxies (Kaiser 2000; Bernstein & Jarvis 2002; Hirata & Seljak 2003a; Dawson et al. 2016); shape bias for blended galaxies (Dawson et al. 2016; Hoekstra et al. 2017; Samuroff et al. 2018; Euclid Collaboration et al. 2019); and increased pixel-noise bias and reduced statistical sensitivity (Sanchez et al. 2021). Additionally, blending impacts galaxy photometry (Huang et al. 2018; Boucaud et al. 2020), and even causes (rare) catastrophic outliers in photometry measurements (Everett et al. 2022). Because blending will occur between galaxies at different redshifts (e.g., Dawson et al. 2016), photometric redshift (photo- z) estimates, which are an essential ingredient of weak lensing cosmological analyses, are impacted by blending (Mandelbaum 2018). Algorithms are already in development for measuring photo- z in the presence of blends (Jones & Heavens 2019a,b). However, more studies are needed to fully understand the impact of blending on photo- z estimation for cosmic shear analyses.

Quantities of interest in cluster cosmology, including total cluster mass and redshifts of member galaxies, provide another important cosmological probe (e.g., Planck Collaboration et al. 2016; Lesci et al. 2022; Abbott et al. 2020; Sunayama et al. 2023; Bocquet et al. 2024; Mantz et al. 2014), as they describe the high density peaks in the mass power spectrum, providing complementary information to the weak lensing results. Galaxy clusters host a particularly high density of galaxies, which increases the rate of blending (Liang 2022); therefore, blending has the potential to bias these important measurements. The best known way to calibrate the total cluster mass is by measuring the weak lensing distortion of background source galaxies (e.g., Metzler et al. 1999). Recent studies show that *recognized* galaxy blends – i.e., blends in which each galaxy member is accurately identified as an individual galaxy – in clusters could bias the weak lensing profile ($\Delta\Sigma(r)$) by about 20% (Ramel et al. 2023), likely due to shape misestimation. One of

the main sources of bias in estimating the cluster mass is the misidentification of cluster members as background galaxies (e.g., Varga et al. 2019). The classification accuracy is strongly dependent upon precise photo- z estimates for cluster member and background galaxies (e.g., Esteves et al. 2024). Blending has the potential to increase the rate of misidentification in two ways: (1) cluster and background galaxies could be blended to the extent that they become unrecognized blends, at which point contamination becomes unavoidable; (2) blending from faint sources could impact the observed colors of galaxies (Gruen et al. 2019), which would bias estimates of photo- z s.

Given the plethora of complicated biases blending can induce in cosmology probes, it is essential to leverage simulations to understand the impact of blending on these probes and to calibrate blending related biases in analyses (Melchior et al. 2021). A widely used package for generating simulated galaxy images is GALSIM (Rowe et al. 2015), which can generate galaxy images for a range of galaxy profiles, point spread functions (PSF), and noise levels. GALSIM has been used to calibrate blending biases for weak lensing (e.g., MacCrann et al. 2022; Dalal et al. 2023), and forms the basis for several large-scale simulations of cosmological surveys. One such simulation emulating LSST observations is the LSST DESC second data challenge (DC2) Simulated Sky Survey (LSST Dark Energy Science Collaboration (LSST DESC) et al. 2021), which uses a full end-to-end approach – starting from N-body cosmological simulations and outputting catalogs based on forward-modeled astronomical images processed by the LSST Science Pipelines. DC2 has already been used to support various blending studies in the context of LSST (Buchanan et al. 2022; Ramel et al. 2023). Finally, another powerful tool is to use multiple surveys with different angular resolutions, such as a ground-based and a space-based survey, to characterize the rate of blending (Mandelbaum et al. 2018; Troxel et al. 2023) or improve deblending (Joseph et al. 2021).

Another approach to mitigating the blending problem is the development and application of *deblenders*: algorithms designed to measure the individual properties of each galaxy in a blend. In principle, an ideal deblender would allow the recovery of these individual properties and the corresponding catalogs could be analyzed ignoring blending altogether. However, in practice, detection and deblending can fail in various ways: blends may not be identified (unrecognized blends), and the deblending process might infer galaxy properties inaccurately depending on the severity of the blend. The former effect can introduce an additional source of systematic error in cosmic shear measurements (Nourbakhsh et al. 2022). SourceExtractor (SExtractor) is an early deblender that uses a thresholding technique for object detection and a multiple isophotal analysis for deblending (Bertin, E. & Arnouts, S. 1996). More modern deblenders use non-parametric constrained optimization techniques (Joseph et al. 2016; Melchior et al. 2018), such as the SCARLET deblender, or machine learning techniques (Arcelin et al. 2021; Hansen et al. 2022; Liu et al. 2023; Merz et al. 2023; Sampson et al. 2024; Biswas et al. 2024).

Despite the range of available simulation packages and deblenders, there is currently no standard framework dedicated to creating customizable simulations of blended galaxies, or comparing the performance of different deblending algorithms using consistent simulated galaxy densities, fluxes, noise levels, image resolutions, etc., and consistent deblending metrics. To address this limitation, we introduce the *Blending Toolkit* (BTK), a modular Python-based software package that leverages GALSIM to generate reproducible and customizable astronom-

ical images of galaxy blends under the observing conditions of several dark energy surveys. BTK also includes a module standardizing existing deblenders such that their outputs can be directly compared against one another when applied to the same images. Finally, our package includes a growing library of deblending metrics to enable evaluation of the performance of deblenders.

We will first describe the design philosophy for BTK in Section 2. Then, we describe the software modules comprising BTK in detail Section 3, followed by an outline of the existing Jupyter Notebook tutorials and documentation in Section 4. We provide a brief summary and outlook for the future in Section 5.

2. DEVELOPMENT APPROACH

The original motivation for BTK was to build a framework that could bring together the various simulation and deblending efforts within the LSST Dark Energy Science Collaboration (DESC) Blending Working Group and the broader cosmology community. We observed a number of ideas for deblenders being developed; however, it was difficult to assess their relative performance compared to existing state-of-the-art deblenders, or their strengths and weaknesses. This was mainly because the majority of deblender studies used a different set of astronomical images (or simulations) and metrics to evaluate their deblenders. In order to make progress in deblender development, a way to assess and benchmark existing deblenders consistently was needed, and this is one of the main purposes of BTK.

BTK is designed to be:

- **Modular:** The simulation, deblending, and metric components of BTK can be connected together to form a full analysis pipeline, as demonstrated in the tutorials available for BTK (see Section 4); however, these components are also designed to be usable independently.
- **Customizable:** Users can customize the various BTK modules to fit their desired blending analysis. For example, the simulations of blended galaxies within BTK contain many options for changing the configuration of galaxy blends (e.g., the rate of blending) or the observing conditions (e.g., noise level or PSF). Comprehensive documentation and examples make it clear how to change the various options within the package.
- **Parallelizable and Reproducible:** Every computationally intensive process in BTK (e.g., producing simulations or running deblenders) can be split across multiple CPUs to improve efficiency. We carefully ensured that all simulations produced by BTK are reproducible given a single random seed. Randomness is propagated using a `numpy.random.SeedSequence` object during multiprocessing to guarantee said reproducibility.
- **Easy-to-Install:** BTK only has a few Python dependencies, the main one being `GALSIM`. This ensures that the package is easily installable with a single `pip` command.

3. STRUCTURE

The overall structure of BTK is summarized in Figure 1. The *Generation* module provides the simulated data containing blended galaxy images, isolated galaxy images, and ground truth properties of galaxies in the blend. Then, with the *Deblending* module, detection or deblending algorithms can

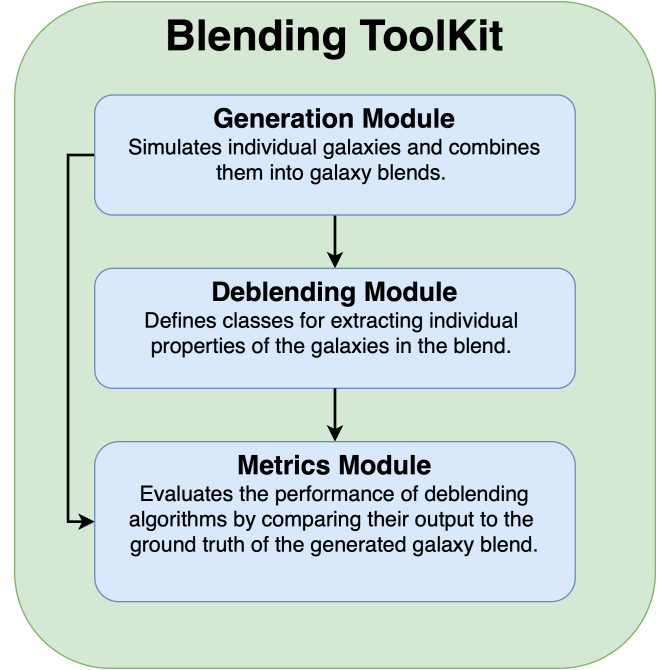


FIG. 1.— **Overall BTK structure.** The software package consists of three main modules: *Generation*, *Deblending*, and *Metrics*. Each arrow indicates the data flow between modules.

be applied to the generated images of galaxy blends. Users can choose to implement their own algorithm or use one of the existing ones in BTK. Finally, in the *Metrics* module, users can evaluate the performance of their detection or deblending algorithms by comparing their output to the ground truth data. This module also contains functionality to perform measurements on the simulated images, including photometry and galaxy shapes, which makes it possible to measure the impact of blending on relevant physical quantities.

3.1. Generation Module

The Generation module renders simulations of galaxy blends that can be used as an input to deblenders for their evaluation. Specifically, this module provides a `DrawBlendsGenerator` class that outputs galaxy blend images in batches i.e., a small collection of objects that can fit in computer memory. This class is implemented as a python generator object, which at each iteration outputs the galaxy blend images, as well as auxiliary galaxy images and truth galaxy catalogs. This generator class also supports multiprocessing to increase the speed of the generation procedure.

Simulated galaxy blends are produced by simulating individual galaxy images with `GALSIM` according to the provided galaxy properties and specified survey observing conditions. Then, these individual galaxy images are combined into a single galaxy blend image, and noise is added. Additionally, the `DrawBlendsGenerator` keeps track of the true properties of every galaxy in each blend, and these properties are returned alongside the galaxy blend images and the (noiseless) images of each individual galaxy. These additional outputs are helpful when evaluating or training deblenders, as is the case for ML-based algorithms. For convenience and validation, the output is handled by the `BlendBatch` class. An outline of the overall structure of this module is presented in Figure 2.

The user can customize the blend generation procedure by modifying the following:

Catalog: The Catalog class standardizes the input information about the galaxies that will be used for rendering. The underlying structure of the catalog is an astropy table (Astropy Collaboration et al. 2013, 2018, 2022), where each row contains information about a given galaxy’s properties such as ellipticity, magnitude in different bands, and size. BTK currently supports two types of catalog formats: CatSim’s parametric catalogs (Connolly et al. 2014) and GALSIM’s COSMOS catalogs (Mandelbaum et al. 2012). Each of these types of catalogs has its dedicated class in BTK.

The CatsimCatalog class used in BTK uses an astropy table containing parameters for simulating galaxies based on a three component model: a bulge, a disk and an AGN¹. Each galaxy has an overall total flux, each component has an associated flux fraction, and the bulge and disk components have independent sizes and ellipticities. All galaxy properties except for the flux are fixed across all LSST bands. The input catalog for this class follows the format used by CatSim (Connolly et al. 2014), which is the earliest version of an end-to-end LSST simulation framework. BTK provides a sample catalog of approximately 85000 galaxies taken from the original CatSim simulation². The galaxy properties from the CatSim catalog were designed to match the key observables in the LSST survey, and are taken from previous studies on galaxy formation and SDSS observations (Bruzual & Charlot 2003; De Lucia et al. 2006; González et al. 2009).

Alternatively, the image-based COSMOS catalog (Mandelbaum et al. 2012) can be used to generate realistic galaxy profiles. The COSMOS catalog consists of about 80,000 galaxies extracted from the Hubble Space Telescope (HST) COSMOS survey (Koekemoer et al. 2007), which are used for the base catalog in GALSIM (Rowe et al. 2015). Currently, the CosmosCatalog class within BTK enables using the COSMOS catalog to render BTK blends by combining multiple GALSIM RealGalaxy profiles that were constructed from HST images.³ When using COSMOS galaxies in a multi-band survey within BTK, the same F814W magnitude is used for all bands, though accounting for the different filters’ zeropoints and exposure times. However, a user may also provide multi-band information, which will then be used by BTK to provide an independent flux in each band. Importantly, this functionality does not account for color gradients within a galaxy profile.

Sampling Function: The sampling functions are customizable functions that select galaxies from a large catalog to form a given output blend, as well as their relative location within the blend. These functions are designed to be flexible, for example, one of the default sampling functions in BTK randomly selects pairs of galaxies in a catalog and outputs 2-galaxy blends with the brightest galaxy fixed to the center of the stamp, while the dimmer galaxy is a uniformly random distance from the central galaxy. Most sampling functions currently implemented support various input parameters that control the degree of blending and total number of galaxies in the galaxy blends produced. Users are additionally encouraged to create their own sampling functions depending on their scientific needs. One of the tutorials, `01-advanced-generation`, detailed in Section 4, provides guidelines and examples on how to achieve

¹ Some galaxies have an Active Galactic Nucleus, which means that their nucleus is much brighter than usual, sometimes as much as the rest of the galaxy.

² <https://www.lsst.org/scientists/simulations/catsim>

³ For more details see https://galsim-developers.github.io/GalSim/_build/html/real_gal.html

this.

Survey: The Survey class contains all information of a given astronomical survey, including the telescope optics, which guarantee that generated images approximately reproduce the observing conditions of the ones observed with that particular survey.

To organize this information, BTK uses SURVEYCODEX⁴, a tiny Python library with referenced survey parameters for the current main galaxy surveys as well as their filters. For more information about SURVEYCODEX and currently supported surveys, see Appendix B. Importantly, the Survey class also contains the point-spread function (PSF) that is applied to galaxies, which can also be easily specified and changed by the user.

Once the catalog, sampling function, and survey are specified, simulated data in the form of BlendBatch objects can be easily generated using the DrawBlendsGenerator class.

3.2. Deblending

In the context of BTK, we refer to a *deblender* as any algorithm that takes as input images of galaxy blends and attempts to output properties of the individual sources (e.g., centroid location) or a reconstruction of the individual galaxies composing the blend.

One of the main goals of BTK is to allow users to test their preferred detection or deblending algorithm in a controlled setting. We provide a framework that enables running such algorithms directly on the BlendBatch output of the Generation module (Section 3.1). The results can then be analyzed by the user separately or compared with other algorithms using a set of BTK built-in blending metrics, as described in Section 3.3. An outline of overall structure of the deblending module is presented in Figure 3.

Our deblender framework is facilitated by the Deblender class, which aims to standardize the inputs and outputs of any given deblending algorithm. The input is always an instance of the BlendBatch class (defined in Section 3.1), and the outputs are structured into the DeblendBatch class containing the following attributes:

1. **Predicted catalog:** contains detection information about each galaxy (i.e., centroid locations), as well as additional optional measurements of galaxy properties.
2. **Deblended images:** contains the reconstruction of each individually detected galaxy.
3. **Segmentation:** contains pixel level segmentation information of the blended image, i.e., for each detected source, and for each pixel of the blended image, a value of 0 or 1 indicating whether the given source contributes flux to that pixel.⁵

Note that not all of these outputs are required as output of a given Deblender subclass. This means that our framework accommodates algorithms that only perform detection or only reconstruction, for instance.

Users are encouraged to contribute to our growing library of BTK deblenders by implementing their own algorithm as a

⁴ <https://github.com/LSSTDESC/surveycodex>

⁵ We opt to use this data format for image segmentation, rather than allowing a more flexible representation with values between 0 and 1 (perhaps corresponding to the fraction of the flux for each source), because our current deblenders and metrics would not take advantage of the additional flexibility.

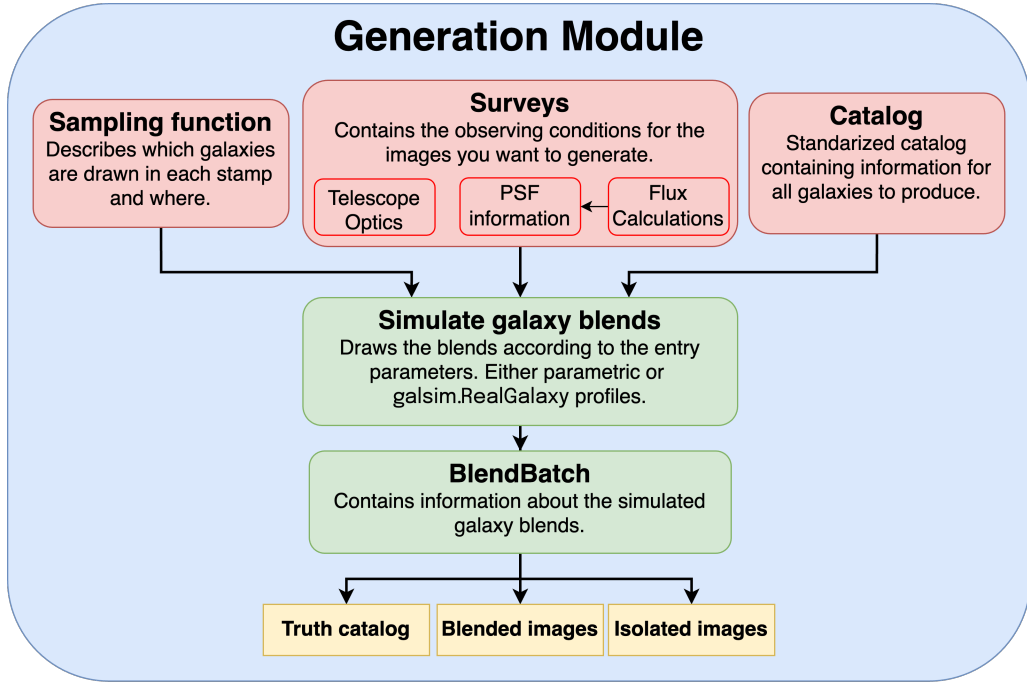


FIG. 2.— **Generation Module of BTK.** This module contains the functionality and configurations for creating galaxy simulations in BTK. The `sampling_function` submodule encodes how galaxies are organized into blends. The `surveys` submodule specifies the observing conditions. Finally, the `catalog` submodule encodes the properties of each individual galaxy. The red blocks are intended to be easily customized by the user, while green blocks are intended to be used ‘as-is’ and can only be modified by advanced users. Yellow blocks indicate the outputs of a given module. See Section 3.1 for more details on this module.

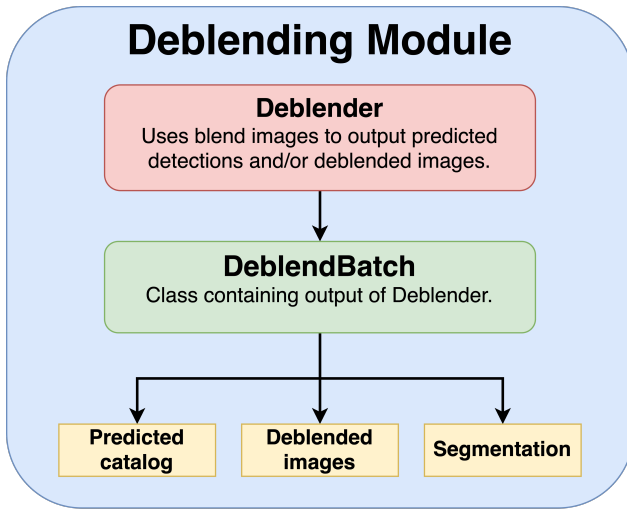


FIG. 3.— **Deblending Module of BTK.** This module contains a standardized library of deblenders that can be used within BTK. The module is designed to allow users to run their preferred detection or deblending algorithm on simulated data from the Generation module of BTK. Additionally, users can implement a new algorithm by creating a new subclass of the `Deblender` class. The output of `Deblender` in BTK is a `DeblendBatch` object, which can contain a predicted catalog, deblended images, and segmentation. See Section 3.2 for more details on this module.

subclass of `Deblender`. This would enable other BTK users to use their deblender and consistently compare with existing ones. We provide several examples of ready-to-use deblenders, and provide tutorials on how this class should be structured.

Currently in BTK, the following deblenders are implemented:

- Peak-finding (van der Walt et al. 2014): Basic algorithm for finding local maxima. It takes as input a target image with one or more light sources, the minimum distance between detected peaks, the minimum intensity of peaks, and the maximum number of peaks that can be

detected. It outputs a detection catalog corresponding to the detected peaks.

- Source Extractor (Bertin, E. & Arnouts, S. 1996; Barbary 2016): We use the python implementation (SEP) of this widely-used software for generating light source catalogs. In the context of BTK, the input to this function is the target image, the minimum distance between matches (in arcseconds), and the minimum pixel value for detection. This algorithm outputs a detection catalog and a segmentation, which is in turn used to provide a basic reconstruction (by extracting the pixels corresponding to the segmentation from the target image).
- SCARLET (Melchior et al. 2018): Deblending algorithm using non-parametric constrained optimization, and which is integrated into the LSST software pipeline. The input includes the detections, the choice of SCARLET models to be optimized for each detection, the PSF, and the noise level. The output is a deblended galaxy reconstruction for each detection.

Specifically, for Source Extractor, we use the SEP (Source Extractor in Python) implementation (Barbary 2016), and the `peak_local_max` function⁶ within `scikit-image` (van der Walt et al. 2014) for the peak-finding algorithm.

3.3. Metrics and Measurement

BTK provides a suite of metrics for evaluating deblending algorithms, which is designed to be applied given the `BlendBatch` and `DeblendBatch` classes outputted from the previous two modules. However, the tutorials and documentation also demonstrate the expected input format for these

⁶ https://scikit-image.org/docs/stable/api/skimage.feature.html#skimage.feature.peak_local_max

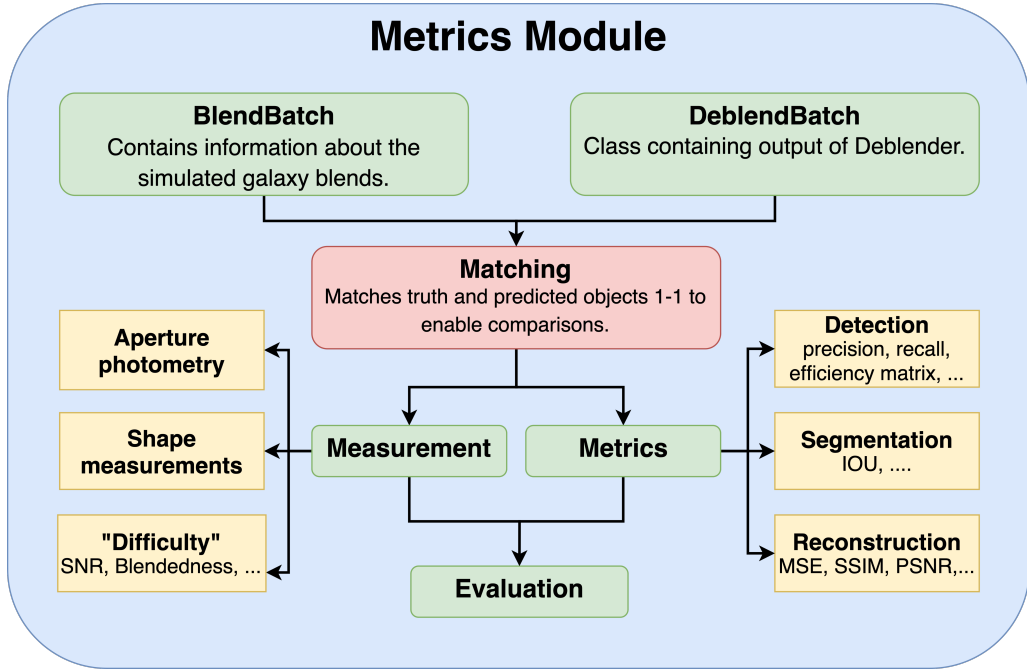


FIG. 4.— **Metrics module of BTK.** This module uses the outputs of the generation module (the ground truth) and the deblender to evaluate the quality of the deblending. Before comparison, the matching module is used to assign true galaxies to detected galaxies and enable the evaluation of residuals. The matched outputs are subjected to various metrics divided in three categories: *detection*, *segmentation*, and *reconstruction*. Finally, the measurement module uses the images or catalogs from BlendBatch or DeblendBatch to compute physical galaxy quantities for analysis including ellipticities, signal-to-noise-ratio (SNR), and blendedness. See Section 3.3 for more details on this module.

metrics, so that they could also be used in isolation from the standard BTK pipeline. An outline of overall structure of this module is also presented in Figure 4.

The BTK metrics are divided into three broad categories:

- **Detection:** These are metrics related to correctly counting the number of galaxies in a given image, as well as the accuracy of the predicted centroid of that galaxy. Examples of these metrics include *precision*, *recall*, and the *efficiency matrix*.
- **Segmentation:** These metrics evaluate the quality of assignments of individual pixels to a corresponding identified source. An example of this metric type is *intersection-over-union* (IoU).
- **Reconstruction:** These metrics relate to the correctness of the individual galaxy images obtained from a given galaxy blend. Examples of this metric type include the *peak signal-to-noise ratio* (PSNR) (Ponomarenko et al. 2011) and the *structural similarity index* (SSIM) (Wang et al. 2004).

We provide a full list of the currently implemented metrics in BTK in Table 1. For each metric, we also provide the corresponding equation and a brief description. Each of these metrics has been used previously at least once in the galaxy deblending literature.

All of the metrics implemented in BTK require information about the correspondence between detections and true sources, i.e., the *matching* between the true and predicted galaxy catalog. In particular, the detection metrics require knowledge of which detections actually correspond to true objects, so that the number of true positives can be computed, while the other two types of metrics compare segmentations or reconstructions of galaxy images in a one-to-one basis. Given that the matching procedure can be subject to different user choices, we provide

this functionality within BTK, through the *Matcher* class, whose implementation through subclasses performs this procedure.

We currently have implemented two different algorithms to perform matching, both of which are based on the relative distances between true centroids and detections, as well as their respective counts. The first implemented matcher is the *PixelHungarianMatcher*, which matches galaxy centroids and detections based on their pixel value. This matcher is based on the Hungarian algorithm (Kuhn 1955), which finds an optimal weight matching in bipartite graphs. We use the implementation available as the SciPy (Virtanen et al. 2020) function `linear_sum_assignment`. The other matcher implemented within BTK is the *SkyClosestNeighbourMatcher*, which performs matching using (ra, dec) coordinates using the `SkyCoord.match_to_catalog_sky` method in Astropy (Astropy Collaboration et al. 2013, 2018, 2022). This method internally uses KD Trees and a nearest neighbor algorithm to output matches. Additional custom matching algorithms can be implemented in BTK creating subclasses of the *Matcher* parent class.

Finally, for additional evaluation of the deblending output, we provide a set of utility functions that can compute “measurements” based on the simulated galaxy images generated by BTK. The output of these measurement functions could be used to further evaluate the reconstruction from deblenders, or to assess the challenge posed by a particular galaxy blend. Currently, BTK provides the following measure functions:

- *Ellipticity measurement* of galaxy shapes using the KSB shear estimator implementation from the `galsim.hsm` module.
- *Aperture Photometry*, we provide a wrapper around the SEP aperture photometry methods to compute aperture photometry fluxes in BTK.
- *Blendedness*, which characterizes the degree to which

the flux from a given light source overlaps with the flux of its neighbors. We use the definition from [Bosch et al. \(2017\)](#).

- *Signal-to-Noise ratio (SNR)*, which characterizes the relative brightness of the source with respect to the noise level of the image. We use the definition in [Arcelin et al. \(2021\)](#).

4. TUTORIALS AND EXAMPLES

We have included comprehensive documentation⁷ in BTK in order to make this package as accessible as possible. In addition to the complete API, it contains a step-by-step user guide, instructions on how to acquire the galaxy catalogs, as well as a set of detailed tutorials with code examples. A code example demonstrating the BTK API is presented in Appendix A. Tutorials are available in the BTK GitHub repository⁸ as Jupyter notebooks. The tutorials start with the basics of using BTK, and progress to advanced applications and customization of the codebase.

4.1. List of tutorials

In this section, we present the current list of tutorials. Note that the numbered prefix of the notebook names indicates relative complexity in increasing order.

- **00-quickstart**: This tutorial is an introduction to BTK, which goes through the entire pipeline of simulating data, deblending, and evaluating results with metrics. It presents the simplest version of the BTK workflow, making it ideal for newcomers to the codebase. More details on each module and customization options are presented in tutorials that follow.
- **01-advanced-generation**: This tutorial is a deeper dive into the generation module (Section 3.1) within BTK and showcases the different types of sampling functions, surveys, and observing condition options. We also demonstrate with examples how users would write their own sampling functions, vary the input PSF, and customize the survey objects. Finally, we also demonstrate how to use COSMOS Real galaxies ([Mandelbaum et al. 2012](#)) option within BTK to simulate galaxies with realistic morphology.
- **01-advanced-deblending**: This tutorial demonstrates usage of all the deblenders currently available within BTK (Section 3.2), including how to customize their hyper-parameters, and what type of output is available from them. Finally, we also show how to run multiple deblenders on the same BTK generated data, which enables consistent comparisons between deblenders.
- **01-advanced-metrics**: This tutorial shows how to use all of the metrics within the metric library of BTK (Section 3.3), as well as explanations for the output, and plots on simple examples to develop intuition. We also demonstrate the measure functions that are available, and how to use them on BTK data products. Finally, we explain in more detail the matching procedure in BTK and the types of matching algorithms that are available.

⁷ <https://lsstdesc.org/BlendingToolKit/>

⁸ <https://github.com/LSSTDESC/BlendingToolKit>

- **02-advanced-analysis**: In this tutorial, we create more complex analysis plots and evaluate multiple deblenders simultaneously within the BTK framework. For example, we demonstrate a comparison of two deblenders applied on the same simulated data that perform detection, and bin their precision and recall metrics by signal-to-noise (SNR). We also demonstrate applying measure functions to the output of the SCARLET deblender to compute the corresponding ellipticity residuals binned by SNR.

4.2. Example analysis plots

The final tutorial 02-advanced-analysis includes a variety of useful evaluation plots involving the use of multiple deblenders and metrics. In this section, we present the plots produced in this notebook as an example of the types of analyses that BTK could facilitate. The exact definition of all the metrics applied to produce the corresponding figures in this section can be found in Table 1.

Dataset: For all of the analysis plots we use the same `DrawBlendsGenerator`, although a different set of blends (random seeds) are used. We choose parametric bulge+disk+AGN blends from the CATSIM catalog for all examples (Section 3.1), where each blend can have anywhere from 0 to 10 galaxies, and the maximum distance of any source from the center of the 120×120 pixel stamp is 15 pixels, which makes blends highly likely. We choose to use the LSST *r*-band survey for all experiments with corresponding parameters presented in Appendix B.2. Finally, we apply an AB magnitude cut of 18 on the bright end and 27 on the dim end.

Deblenders: In terms of the specific settings or hyper-parameters of the deblenders used, these are as follows for all experiments:

- *Scarlet*: We use exactly the same default settings as those in the SCARLET quick start guide⁹.
- *SEP*: We use a `thresh` parameter of 1.5 and `min_area` of 3 pixels with the `sep.extract` function¹⁰, which are close to known reasonable settings for galaxy detection and photometry (e.g., [Sanchez et al. 2021](#)). We allow SEP to measure the background of each stamp and use this for the corresponding noise variance. Otherwise, we use the default SEP parameters.
- *Peak-finder*: We setup the `peak_local_max` algorithm with a `threshold` argument of five sigma above the noise level, and a `min_distance` argument of twice the PSF FWHM.

First, we compare the detection efficiency of `SourceExtractor` in Python (SEP) and the peak-finding algorithm from `scikit-image`. Both of the efficiency matrices are displayed in Figure 5, where the top matrix corresponds to peak-finding and the bottom to SEP. The efficiency matrices have been computed by accumulating the counts from a total of 1000 blends, and normalizing each column by the sum of that column. The colorbar in the figure thus goes from 0 (fully white) to 1 (fully black), where 0 for a given cell (i, j) means that for blends containing j galaxies, the deblender reported i (matched) detections 0 times. Similarly, a value of 1 for a cell (i, j) means

⁹ <https://pmelchior.github.io/scarlet/0-quickstart.html>

¹⁰ <https://sep.readthedocs.io/en/stable/api/sep.extract.html#sep.extract>

Metric	Type	Equation	Description
Precision	Detection	$p = \text{TP}/P$	The number of detections that are matched to sources (TP) divided by the total number of detections (P). It represents the quality of detections.
Recall	Detection	$r = \text{TP}/T$	The number of detections that are matched to sources (TP) divided by the total number of true sources (T). It represents the fraction of sources successfully detected.
F1-score	Detection	$F_1 = 2 \cdot (r^{-1} + p^{-1})^{-1}$	Harmonic mean between precision p and recall r , which symmetrically represents both in one metric.
Efficiency Matrix	Detection	E_{ij}	The i -th, j -th element of this matrix is the number of times that i number of galaxies were detected and matched in a blend containing j true galaxies.
Intersection-over-Union	Segmentation	$\text{IoU} = \frac{S_{\text{true}} \cap S_{\text{pred}}}{S_{\text{true}} \cup S_{\text{pred}}}$	Ratio of the intersection area between the true S_{true} and predicted S_{pred} segmentation and their union area.
Mean-squared-error	Reconstruction	$\text{MSR} = \frac{1}{N} \sum_{i=0}^N (x_i^{\text{true}} - x_i^{\text{pred}})^2$	The mean squared residual between the true x^{true} and the reconstructed x^{pred} image, where N is number of pixels in the images.
Peak Signal-to-Noise ratio	Reconstruction	$\text{PSNR} = \log(M/\text{MSR}^2)$	The ratio between the maximum power of the signal (M) and the corrupting noise (MSR^2).
Structural Similarity Index	Reconstruction	$\text{SSIM} = l \cdot c \cdot s$	A more nuanced measure of similarity accounting for the luminance l , the contrast c , and the structure s when comparing two images. (See Wang et al. (2004) for details.)

TABLE 1
METRICS WITHIN BTK. LIST OF ALL THE METRICS AVAILABLE ALONG WITH THEIR TYPE, EQUATION, AND A SHORT DESCRIPTION.

that the deblender reported the correct number of (matched) detections 100% of the times for blends containing j galaxies. We can see from the efficiency matrices that SEP is overall better than the peak-finding algorithm at detection sources in the blends we simulated, as the gray squares in the SEP efficiency matrix is closer to the diagonal. Moreover, SEP is able to detect up to 6 sources in blends with more than 8 galaxies whereas the peak-finding algorithm reaches a maximum of 4 accurate detection across blends of all sizes.

Next, in Figure 6 we show the recall performance of each of these two detection algorithms as a function of the minimum true SNR of the galaxies in a given blend. The recall is computed by taking the number of detections that are matched with true galaxies that have SNR higher than the threshold, and dividing by the number of true galaxies with SNR higher than the threshold. For both the SEP and peak-finding deblenders, we see that as the minimum SNR threshold is increased, the recall increases. This is expected as we are excluding fainter objects as the threshold increases. However, we do not expect to achieve perfect recall even at very high SNRs due to blending. This is indeed what we see for both algorithms, as they both reach only approximately 0.9 recall in the brightest bin. In terms of the relative performance between SEP and the peak-finder deblenders, we see that SEP dominates in terms of recall throughout all SNR bins, but the difference is more pronounced for the bins that include the most dim sources. This is reasonable, as Source Extractor’s thresholding approach is more suitable for detecting faint sources, where as peak-finding is more appropriate for bright, non-diffused light sources. Note that we do not include the corresponding precision plots as for both algorithms the precision is essentially 1.0 for the entire range of SNRs.

Third, in Figure 7 we show three histograms corresponding to the reconstruction metrics available within BTK (see Table 1), comparing SEP and the SCARLET deblender. Each of the histograms is composed of the metric applied to the reconstructions of true galaxies that were detected and matched by the SEP detection algorithm (since SCARLET does not perform detection). The SEP’s reconstruction of a given galaxy is obtained by multiplying the pixel-wise segmentation outputted

by SEP with the galaxy blend image. Overall, we see from the three histograms that SCARLET’s reconstructions are higher quality than SEP’s reconstructions. For instance, the Mean-Squared Error (MSE) between SCARLET’s reconstructions and the true noiseless individual galaxy images are closer to zero on average than SEP’s reconstructions are. Moreover, the structure similarity index is closer to 1 on average for SCARLET, indicating higher visual similarity than SEP’s reconstructions. Both of these results are expected as SCARLET uses a more sophisticated constrained matrix factorization procedure to deblend light sources than SEP.

In Figure 8 we show the residuals between HSM ellipticity¹¹ measured on reconstructions of individual galaxies from SCARLET and on the true individual galaxy images binned by SNR, blendedness (B), and HSM ellipticity measured on the true galaxy images ($e_{1,2}^{\text{true}}$). For this figure, we condition SCARLET on the true centroids of every galaxy in the blend, thus ignoring the effect of unrecognized blends. In each figure, the curve and points correspond to the mean value of each bin, and the shaded bands correspond to the error on the mean for that bin ($\sigma/\sqrt{N_{\text{bin}}}$, where σ is the residual scatter in the bin and N_{bin} is the number of galaxies in that bin). For the ellipticity residual as a function of SNR, we see essentially unbiased reconstructed ellipticity with scatter increasing for decreasing SNR. For blendedness, we see large scatters in the mean residual for some of the bins, which suggests that a couple of outliers are driving the large deviations from mean. Finally, for the functions binned by ellipticity, we see a significant dependence on the mean residual as a function of true ellipticity.

We note that the galaxy blend dataset used in Figure 8 is very strongly blended, and, as stated above, we run SCARLET using the default settings from its basic tutorial. Therefore, this figure might not necessarily be representative of the performance of SCARLET on future survey data. Additionally, the mean of HSM shape measurements is designed to be unbiased (to some degree) only in the case of a small shear applied to a galaxy population with an isotropic distribution of ellipticities. Thus,

¹¹ Specifically, we are using the ‘KSB’ method within the HSM module in GALSIM ([Hirata & Seljak 2003b](#)).

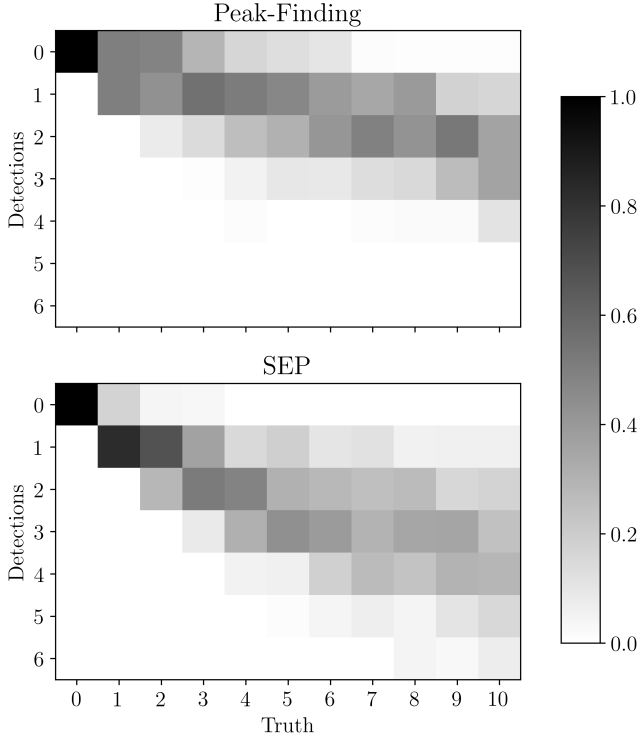


FIG. 5.— **Efficiency matrices of SEP and Peak-finding debenders.** In this plot we show the efficiency matrices (as defined in Table 1) for the SEP and Peak-finding debenders implemented in BTK applied to the dataset of CATSIM blends detailed in Section 4.2. The rows correspond to the number of detections and the columns to the true number of sources in a blend. Each cell of each matrix represents the fraction of times that each debender predicted the row number of detections for the column number of true sources in a blend. See Section 4.2 for more details on this figure.

we do not expect this residual mean to be unbiased as a function of ellipticity even in the case of no blending.

Lastly, in Figure 9 we show an example of a galaxy blend, the true image of each member galaxy, and the respective reconstructions from SCARLET (using the true galaxy centroid as input). We see how the reconstruction of a given individual galaxy can suffer from significant artifacts when it is highly blended or when its SNR is low.

5. SUMMARY

In this paper, we have introduced BTK, an open source package that provides customizable galaxy blends, a standardized framework for deblenders, and a library of deblending metrics that enables self-consistent comparisons. We developed BTK in the context of the Blending Working Group in LSST DESC, in order to further enable the development of deblenders within the collaboration. However, we anticipate that BTK will be useful to anyone interested in analyzing the systematic errors that blending induces in measurements of astronomical sources.

BTK also provides many useful subroutines for understanding galaxy blends and enable an end-to-end analysis. For instance, we provide a `match` module that provides various (customizable) ways of assigning true objects to detections for evaluating the *accuracy* of the reconstruction. This tends to be a subtle step when evaluating deblenders that is performed differently by different studies. Standardizing this step with its own module within BTK allows for more principled comparisons between deblenders. Additionally, BTK provides several utility functions for extracting measured quantities of individual galaxies or blends that are of interest for blending

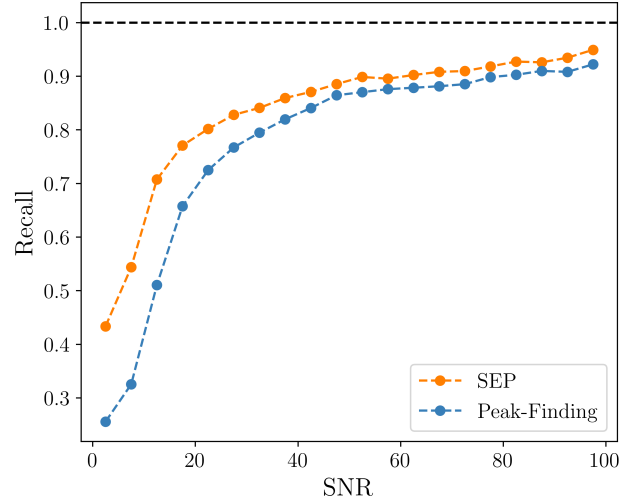


FIG. 6.— **Recall as a function of SNR for SEP and Peak-finding.** In this figure, we compare the achieved recall (as defined in Table 1) by the peak-finding (blue) and SEP (orange) deblenders as a function of the minimum SNR of true galaxies applied to the same CATSIM blend dataset as Figure 5. Note that we exclude the accompanying precision curves as it has approximately a value of 1.0 for all SNRs for both deblenders. See Section 4.2 for more details on this figure.

analyses. These quantities include aperture photometry flux and blendedness. Standardized functions that extract these quantities given BTK output facilitates downstream analyses.

As described in more detail in Section 2, BTK is an open source package hosted on GitHub, and we strive to maintain a culture of open collaboration and development. Anyone interested in galaxy blending is invited to contribute to this package. We have comprehensively tested and documented the software in preparation of the first formal release of the package, v1.0, which accompanies this publication. Finally, we hope that this package and its tutorial suite serve as a pedagogical resource for those interested in learning the basics of blending analysis and deblenders.

The simulations generated by BTK are actively used by the LSST DESC community to test various deblenders in development (Merz et al. 2023; Biswas et al. 2024), and efforts are underway to integrate some of these deblenders into the `deblender` module within BTK. The development of BTK continues after this first release of the software and some future directions include: improving the overall realism of galaxy simulations, expanding the metrics library to allow more types of science analysis beyond those involving galaxy fluxes and shapes, and incorporating more modern galaxy catalogs such as those from the DC2 simulation (LSST Dark Energy Science Collaboration (LSST DESC) et al. 2021).

6. AUTHOR CONTRIBUTIONS

IM was the lead developer and maintainer of the codebase. IM, AT, and TS wrote the paper, created and polished figures, and developed tutorials. IM and TS documented the codebase, developed unit tests, and were co-leads of the BTK team within LSST-DESC. AG gave extensive and detailed guidance on codebase development and structure. AG, CA, EA, and CR were mentors for the primary codebase contributors. AB was the lead developer of SURVEYCODEX, and MP and HM contributed to this codebase. IM, AT, TS, AG, MP, CA, BB, CD, RJ, AIM, HM, and TZ brainstormed and planned BTK codebase development. IM, AT, TS, AB, MP, PA, BB, CD, RJ, SK, and TZ contributed to the codebase. IM, AT, TS, AG,

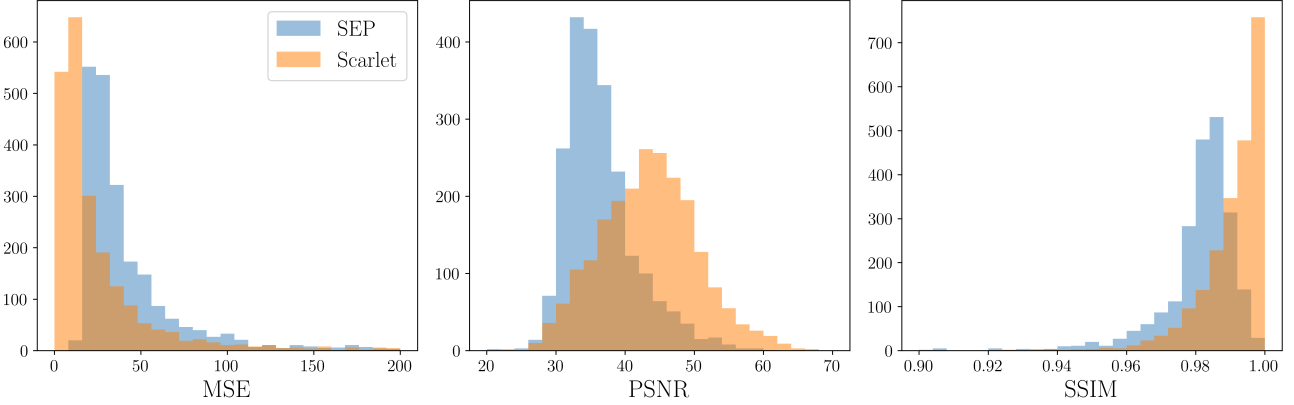


FIG. 7.— **Reconstruction metrics of SEP and Scarlet.** In this figure we show three histogram plots for each of the reconstruction metrics available in BTK: mean-squared error (MSE), peak SNR (PSNR), and structural similarity index (SSIM), as defined in Table 1 for the dataset of CATSIM blends detailed in Section 4.2. The light blue histogram in each plot corresponds to the metrics evaluated on reconstructions of galaxies from the SEP deblender, whereas the orange histogram corresponds to the SCARLET deblender. Each count of each histogram corresponds to the given metric computed from the reconstruction of either SEP or SCARLET of a given detection that was matched to a true galaxy centroid. See Section 4.2 for more details on this figure.

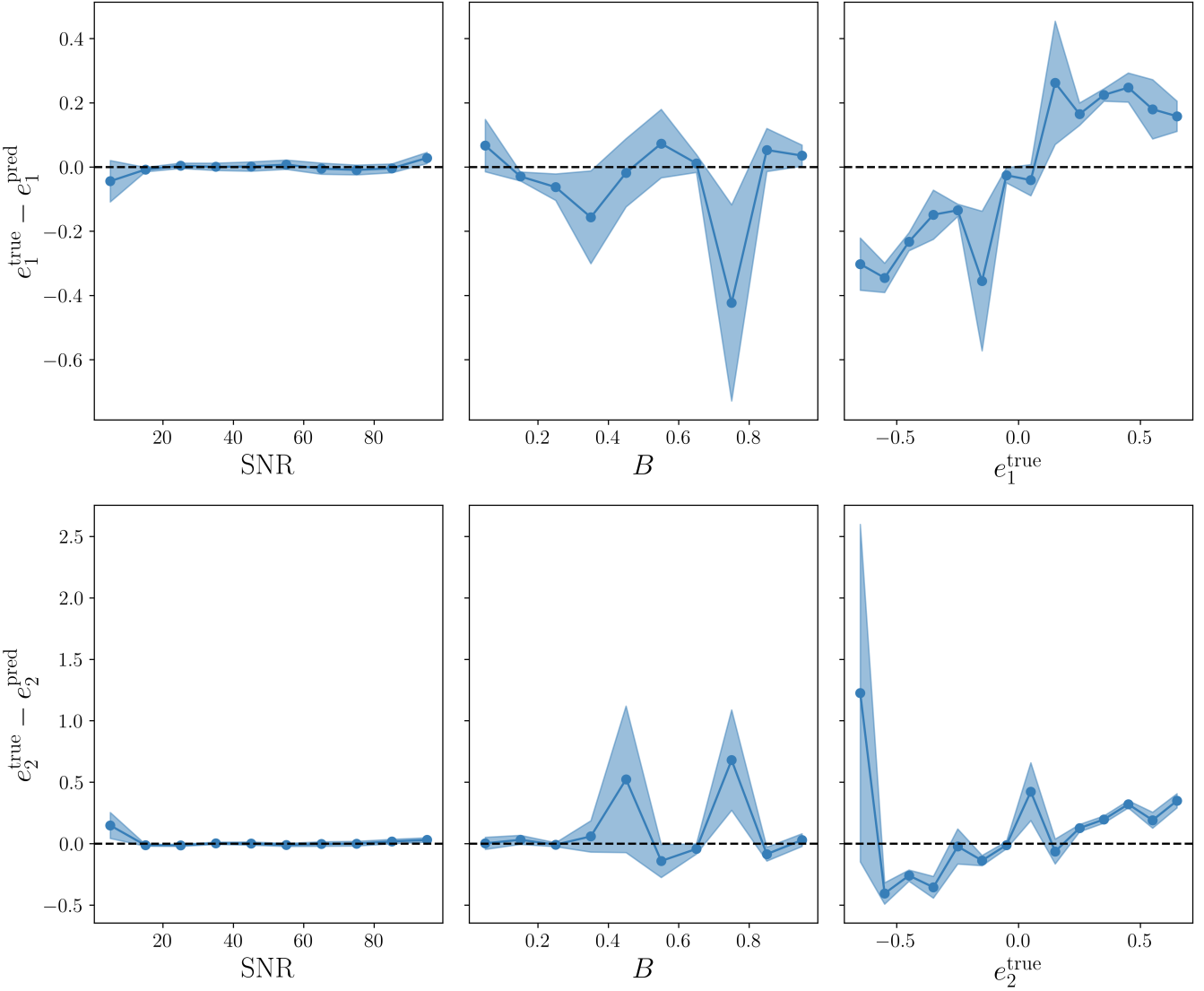


FIG. 8.— **Ellipticity residuals of Scarlet deblender.** In this figure we show the HSM ellipticity residuals between the reconstructed individual galaxies from SCARLET and the true isolated galaxy images binned by signal-to-noise ratio (SNR), blendedness (B), and true measured ellipticity (e_1^{true}). The curve refers to the mean value for that bin and shaded region corresponds to the error on the mean. We emphasize that the dataset of galaxy blends used for this example is strongly blended, so that these plots might not be representative of the performance of SCARLET on future data. See Section 4.2 for more details on this figure.

MP, PA, BB, GM, and TZ identified and fixed bugs within the codebase. IM, AT, TS, and AB performed code reviews for the codebase. MP incorporated “Real” Galsim galaxies into BTK. AG, AB, CA, JB, PB, RJ, and GM gave paper suggestions, edits, and helped improved paper structure. EA, PB, CD, SK, and CR were involved in the initial planning and conception of BTK. JB and TZ managed the working-group in DESC that the BTK team was part of. SK developed the first draft of the codebase.

7. ACKNOWLEDGEMENTS

This paper has undergone internal review in the LSST Dark Energy Science Collaboration. We are grateful to our internal reviewers, Mike Jarvis and Shuang Liang, for their thoughtful feedback.

IM and CA acknowledge support from DOE grant DE-SC009193. IM acknowledges the support of the Special Interest Group on High Performance Computing (SIGHPC) Computational and Data Science Fellowship. IM acknowledges support from the Michigan Institute for Computational Discovery and Engineering (MICDE) Graduate Fellowship. IM acknowledges support from the LSSTC Enabling Science Award. IM acknowledges support from the Leinweber Center for Theoretical Physics Summer Fellowship. AIM acknowledges the support of Schmidt Sciences. MP and HM acknowledge supports from Japan Society for the Promotion of Science (JSPS) KAKENHI Grant Numbers JP20H01932 and JP23H00108, and Japan Science and Technology Agency (JST) CREST Grant Number JPMHCR1414 and FOREST Program Grant Number JPMJFR2137. GM acknowledges support from NSF grant AST-2308174 and LSST-DA through grant 2023-SFF-LFI-03-Liu. BB acknowledges support from Agence Nationale de la Recherche grant ANR-19-CE23-0024 — AstroDeep, and the European Union’s Horizon 2020 research and innovation pro-

gram under the Marie Skłodowska-Curie grant agreement No 945304 – COFUND AI4theSciences hosted by PSL University.

The DESC acknowledges ongoing support from the Institut National de Physique Nucléaire et de Physique des Particules in France; the Science & Technology Facilities Council in the United Kingdom; and the Department of Energy, the National Science Foundation, and the LSST Corporation in the United States. DESC uses resources of the IN2P3 Computing Center (CC-IN2P3–Lyon/Villeurbanne - France) funded by the Centre National de la Recherche Scientifique; the National Energy Research Scientific Computing Center, a DOE Office of Science User Facility supported by the Office of Science of the U.S. Department of Energy under Contract No. DE-AC02-05CH11231; STFC DiRAC HPC Facilities, funded by UK BEIS National E-infrastructure capital grants; and the UK particle physics grid, supported by the GridPP Collaboration. This work was performed in part under DOE Contract DE-AC02-76SF00515.

We also acknowledge the use of `numpy` (Harris et al. 2020), `scipy` (Virtanen et al. 2020), `scikit-learn` (Pedregosa et al. 2011), `scikit-image` (van der Walt et al. 2014), `astropy` (Astropy Collaboration et al. 2013, 2018, 2022), `matplotlib` (Hunter 2007), `fast3tree`¹², `tqdm`¹³, `h5py`¹⁴, and `GALSIM` (Rowe et al. 2015).

DATA AVAILABILITY

The BlendingToolKit (BTK) is a publicly available package on GitHub at the following link: <https://github.com/LSSTDESC/BlendingToolKit>. Our software is also publicly available in Zenodo at <https://zenodo.org/records/13351808>.

REFERENCES

Abbott, T. M. C., Aguena, M., Alarcon, A., et al. 2020, Phys. Rev. D, 102, 023509, doi: [10.1103/PhysRevD.102.023509](https://doi.org/10.1103/PhysRevD.102.023509)

Aihara, H., Arimoto, N., Armstrong, R., et al. 2018, PASJ, 70, S4, doi: [10.1093/pasj/psx066](https://doi.org/10.1093/pasj/psx066)

Arcelin, B., Doux, C., Aubourg, E., Roucelle, C., & LSST Dark Energy Science Collaboration. 2021, MNRAS, 500, 531, doi: [10.1093/mnras/staa3062](https://doi.org/10.1093/mnras/staa3062)

Astropy Collaboration, Robitaille, T. P., Tollerud, E. J., et al. 2013, A&A, 558, A33, doi: [10.1051/0004-6361/201322068](https://doi.org/10.1051/0004-6361/201322068)

Astropy Collaboration, Price-Whelan, A. M., Sipőcz, B. M., et al. 2018, AJ, 156, 123, doi: [10.3847/1538-3881/aabc4f](https://doi.org/10.3847/1538-3881/aabc4f)

Astropy Collaboration, Price-Whelan, A. M., Lim, P. L., et al. 2022, ApJ, 935, 167, doi: [10.3847/1538-4357/ac7c74](https://doi.org/10.3847/1538-4357/ac7c74)

Barbary, K. 2016, Journal of Open Source Software, 1, 58, doi: [10.21105/joss.00058](https://doi.org/10.21105/joss.00058)

Bernstein, G. M., & Jarvis, M. 2002, AJ, 123, 583, doi: [10.1086/338085](https://doi.org/10.1086/338085)

Bertin, E., & Arnouts, S. 1996, Astron. Astrophys. Suppl. Ser., 117, 393, doi: [10.1051/aa:1996164](https://doi.org/10.1051/aa:1996164)

Biswas, B., Aubourg, E., Boucaud, A., et al. 2024, MADNESS Deblender: Maximum A posteriori with Deep NEural networks for Source Separation. <https://arxiv.org/abs/2408.15236>

Bocquet, S., Grandis, S., Bleem, L. E., et al. 2024, SPT Clusters with DES and HST Weak Lensing. II. Cosmological Constraints from the Abundance of Massive Halos. <https://arxiv.org/abs/2401.02075>

Bosch, J., Armstrong, R., Bickerton, S., et al. 2017, Publications of the Astronomical Society of Japan, 70, doi: [10.1093/pasj/psx080](https://doi.org/10.1093/pasj/psx080)

Boucaud, A., Huertas-Company, M., Heneka, C., et al. 2020, MNRAS, 491, 2481, doi: [10.1093/mnras/stz3056](https://doi.org/10.1093/mnras/stz3056)

¹² <https://github.com/yymao/fast3tree>

¹³ <https://github.com/tqdm/tqdm>

¹⁴ <https://github.com/h5py/h5py>

Bruzual, G., & Charlot, S. 2003, Monthly Notices of the Royal Astronomical Society, 344, 1000

Buchanan, J. J., Schneider, M. D., Armstrong, R. E., et al. 2022, ApJ, 924, 94, doi: [10.3847/1538-4357/ac35ca](https://doi.org/10.3847/1538-4357/ac35ca)

Chang, C., Jarvis, M., Jain, B., et al. 2013, MNRAS, 434, 2121, doi: [10.1093/mnras/stt1156](https://doi.org/10.1093/mnras/stt1156)

—. 2015, MNRAS, 447, 1746, doi: [10.1093/mnras/stu2553](https://doi.org/10.1093/mnras/stu2553)

Connolly, A. J., Angeli, G. Z., Chandrasekharan, S., et al. 2014, in Society of Photo-Optical Instrumentation Engineers (SPIE) Conference Series, Vol. 9150, Modeling, Systems Engineering, and Project Management for Astronomy VI, ed. G. Z. Angeli & P. Dierickx, 915014, doi: [10.1117/12.2054953](https://doi.org/10.1117/12.2054953)

Cuillandre, J. C., & Bertin, E. 2006, in SF2A-2006: Semaine de l’Astrophysique Francaise, ed. D. Barret, F. Casoli, G. Lagache, A. Lecavelier, & L. Pagani, 265

Dalal, R., Li, X., Nicola, A., et al. 2023, Phys. Rev. D, 108, 123519, doi: [10.1103/PhysRevD.108.123519](https://doi.org/10.1103/PhysRevD.108.123519)

Dark Energy Survey Collaboration, Abbott, T., Abdalla, F. B., et al. 2016, MNRAS, 460, 1270, doi: [10.1093/mnras/stw641](https://doi.org/10.1093/mnras/stw641)

Dawson, W. A., Schneider, M. D., Tyson, J. A., & Jee, M. J. 2016, ApJ, 816, 11, doi: [10.3847/0004-637X/816/1/11](https://doi.org/10.3847/0004-637X/816/1/11)

De Lucia, G., Springel, V., White, S. D., Croton, D., & Kauffmann, G. 2006, Monthly Notices of the Royal Astronomical Society, 366, 499

Eckert, K., Bernstein, G. M., Amara, A., et al. 2020, MNRAS, 497, 2529, doi: [10.1093/mnras/staa2133](https://doi.org/10.1093/mnras/staa2133)

Esteves, J. H., Pereira, M. E. S., Soares-Santos, M., et al. 2024, arXiv e-prints, arXiv:2401.12049, doi: [10.48550/arXiv.2401.12049](https://doi.org/10.48550/arXiv.2401.12049)

Euclid Collaboration, Martinet, N., Schrabback, T., et al. 2019, A&A, 627, A59, doi: [10.1051/0004-6361/201935187](https://doi.org/10.1051/0004-6361/201935187)

Everett, S., Yanny, B., Kuropatkin, N., et al. 2022, ApJS, 258, 15, doi: [10.3847/1538-4365/ac26c1](https://doi.org/10.3847/1538-4365/ac26c1)

González, J. E., Lacey, C., Baugh, C., Frenk, C., & Benson, A. 2009, Monthly Notices of the Royal Astronomical Society, 397, 1254

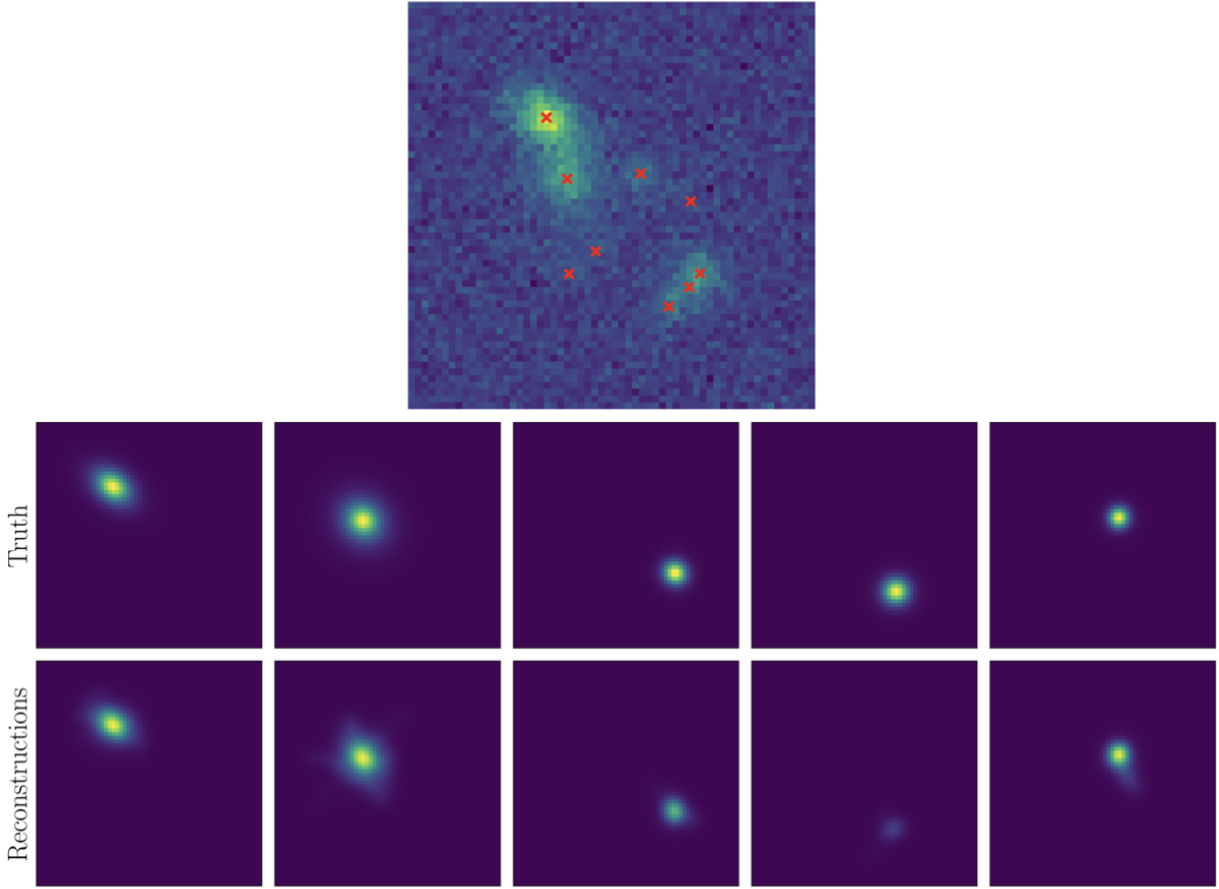


FIG. 9.— **Example of Scarlet Reconstructions.** In this figure we showcase an example of a galaxy blend image (top, middle) with the centroid of each galaxy marked in red, and the true (noiseless) image of each individual galaxy (top row) along with the respective SCARLET reconstruction (bottom row). Each of the galaxies are ordered by total flux from left to right, and their positions are the same as in the original blend.

Gruen, D., Zhang, Y., Palmese, A., et al. 2019, MNRAS, 488, 4389, doi: [10.1093/mnras/stz2036](https://doi.org/10.1093/mnras/stz2036)

Hansen, D. L., Mendoza, I., Liu, R., et al. 2022, in Machine Learning for Astrophysics, 27, doi: [10.48550/arXiv.2207.05642](https://doi.org/10.48550/arXiv.2207.05642)

Harris, C. R., Millman, K. J., van der Walt, S. J., et al. 2020, Nature, 585, 357, doi: [10.1038/s41586-020-2649-2](https://doi.org/10.1038/s41586-020-2649-2)

Hartlap, J., Hilbert, S., Schneider, P., & Hildebrandt, H. 2011, A&A, 528, A51, doi: [10.1051/0004-6361/201015850](https://doi.org/10.1051/0004-6361/201015850)

Hirata, C., & Seljak, U. 2003a, MNRAS, 343, 459, doi: [10.1046/j.1365-8711.2003.06683.x](https://doi.org/10.1046/j.1365-8711.2003.06683.x)

—. 2003b, MNRAS, 343, 459, doi: [10.1046/j.1365-8711.2003.06683.x](https://doi.org/10.1046/j.1365-8711.2003.06683.x)

Hoekstra, H., Viola, M., & Herbonnet, R. 2017, MNRAS, 468, 3295, doi: [10.1093/mnras/stx724](https://doi.org/10.1093/mnras/stx724)

Huang, S., Leauthaud, A., Murata, R., et al. 2018, PASJ, 70, S6, doi: [10.1093/pasj/psx126](https://doi.org/10.1093/pasj/psx126)

Hunter, J. D. 2007, Computing in Science & Engineering, 9, 90, doi: [10.1109/CMSE.2007.55](https://doi.org/10.1109/CMSE.2007.55)

Huterer, D. 2002, Physical Review D, 65, 063001

Ivezic, Z., Kahn, S. M., Tyson, J. A., et al. 2019, ApJ, 873, 111, doi: [10.3847/1538-4357/ab042c](https://doi.org/10.3847/1538-4357/ab042c)

Jones, D. M., & Heavens, A. F. 2019a, MNRAS, 483, 2487, doi: [10.1093/mnras/sty3279](https://doi.org/10.1093/mnras/sty3279)

—. 2019b, MNRAS, 490, 3966, doi: [10.1093/mnras/stz2687](https://doi.org/10.1093/mnras/stz2687)

Joseph, R., Courbin, F., & Starck, J.-L. 2016, Astronomy & Astrophysics, 589, A2

Joseph, R., Melchior, P., & Moolekamp, F. 2021, arXiv e-prints, arXiv:2107.06984, doi: [10.48550/arXiv.2107.06984](https://doi.org/10.48550/arXiv.2107.06984)

Kaiser, N. 2000, ApJ, 537, 555, doi: [10.1086/309041](https://doi.org/10.1086/309041)

Kilbinger, M. 2015, Reports on Progress in Physics, 78, 086901, doi: [10.1088/0034-4885/78/8/086901](https://doi.org/10.1088/0034-4885/78/8/086901)

Koekemoer, A. M., Aussel, H., Calzetti, D., et al. 2007, ApJS, 172, 196, doi: [10.1086/520086](https://doi.org/10.1086/520086)

Kuhn, H. W. 1955, Naval Research Logistics Quarterly, 2, 83, doi: <https://doi.org/10.1002/nav.3800020109>

Laureijs, R., Gondoin, P., Duvet, L., et al. 2012, in Society of Photo-Optical Instrumentation Engineers (SPIE) Conference Series, Vol. 8442, Space Telescopes and Instrumentation 2012: Optical, Infrared, and Millimeter Wave, ed. M. C. Clampin, G. G. Fazio, H. A. MacEwen, & J. Oschmann, Jacobus M., 84420T, doi: [10.1117/12.926496](https://doi.org/10.1117/12.926496)

Lesci, G. F., Marulli, F., Moscardini, L., et al. 2022, A&A, 659, A88, doi: [10.1051/0004-6361/202040194](https://doi.org/10.1051/0004-6361/202040194)

Liang, S. 2022, PhD thesis, SUNY Stony Brook, New York

Liu, R., McAuliffe, J. D., Regier, J., & The LSST Dark Energy Science Collaboration. 2023, Journal of Machine Learning Research

LSST Dark Energy Science Collaboration (LSST DESC), Abolfathi, B., Alonso, D., et al. 2021, ApJS, 253, 31, doi: [10.3847/1538-4365/abd62c](https://doi.org/10.3847/1538-4365/abd62c)

MacCrann, N., Becker, M. R., McCullough, J., et al. 2022, MNRAS, 509, 3371, doi: [10.1093/mnras/stab2870](https://doi.org/10.1093/mnras/stab2870)

Mandelbaum, R. 2018, ARA&A, 56, 393, doi: [10.1146/annurev-astro-081817-051928](https://doi.org/10.1146/annurev-astro-081817-051928)

Mandelbaum, R., Lackner, C., Leauthaud, A., & Rowe, B. 2012, COSMOS real galaxy dataset, Zenodo, doi: [10.5281/zenodo.3242143](https://doi.org/10.5281/zenodo.3242143)

Mandelbaum, R., Lanusse, F., Leauthaud, A., et al. 2018, Monthly Notices of the Royal Astronomical Society, 481, 3170, doi: [10.1093/mnras/sty2420](https://doi.org/10.1093/mnras/sty2420)

Mantz, A. B., von der Linden, A., Allen, S. W., et al. 2014, Monthly Notices of the Royal Astronomical Society, 446, 2205, doi: [10.1093/mnras/stu2096](https://doi.org/10.1093/mnras/stu2096)

Melchior, P., Joseph, R., Sanchez, J., MacCrann, N., & Gruen, D. 2021, Nature Reviews Physics, 3, 712

Melchior, P., Moolekamp, F., Jerdee, M., et al. 2018, Astronomy and Computing, 24, 129, doi: [10.1016/j.ascom.2018.07.001](https://doi.org/10.1016/j.ascom.2018.07.001)

Merz, G., Liu, Y., Burke, C. J., et al. 2023, MNRAS, 526, 1122, doi: [10.1093/mnras/stad2785](https://doi.org/10.1093/mnras/stad2785)

Metzler, C. A., White, M., Norman, M., & Loken, C. 1999, ApJ, 520, L9, doi: [10.1086/312144](https://doi.org/10.1086/312144)

Nourbakhsh, E., Tyson, J. A., Schmidt, S. J., & LSST Dark Energy Science Collaboration. 2022, MNRAS, 514, 5905, doi: [10.1093/mnras/stac1303](https://doi.org/10.1093/mnras/stac1303)

Pedregosa, F., Varoquaux, G., Gramfort, A., et al. 2011, Journal of Machine Learning Research, 12, 2825

Planck Collaboration, Ade, P. A. R., Aghanim, N., et al. 2016, A&A, 594, A24, doi: [10.1051/0004-6361/201525833](https://doi.org/10.1051/0004-6361/201525833)

Ponomarenko, N., Ieremeiev, O., Lukin, V., Egiazarian, K., & Carli, M. 2011, in 2011 11th International Conference The Experience of Designing and Application of CAD Systems in Microelectronics (CADSM), 305–311

Ramel, M., Doux, C., & Kuna, M. 2023, arXiv e-prints, arXiv:2310.02079, doi: [10.48550/arXiv.2310.02079](https://doi.org/10.48550/arXiv.2310.02079)

Rowe, B. T. P., Jarvis, M., Mandelbaum, R., et al. 2015, Astronomy and Computing, 10, 121, doi: [10.1016/j.ascom.2015.02.002](https://doi.org/10.1016/j.ascom.2015.02.002)

Sampson, M. L., Melchior, P., Ward, C., & Birmingham, S. 2024, arXiv e-prints, arXiv:2401.07313, doi: [10.48550/arXiv.2401.07313](https://doi.org/10.48550/arXiv.2401.07313)

Samuroff, S., Bridle, S. L., Zuntz, J., et al. 2018, MNRAS, 475, 4524, doi: [10.1093/mnras/stx3282](https://doi.org/10.1093/mnras/stx3282)

Sanchez, J., Mendoza, I., Kirkby, D. P., Burchat, P. R., et al. 2021, Journal of Cosmology and Astroparticle Physics, 2021, 043

Sunayama, T., Miyatake, H., Sugiyama, S., et al. 2023, Optical Cluster Cosmology with SDSS redMaPPer clusters and HSC-Y3 lensing measurements. <https://arxiv.org/abs/2309.13025>

Troxel, M. A., Lin, C., Park, A., et al. 2023, MNRAS, 522, 2801, doi: [10.1093/mnras/stad664](https://doi.org/10.1093/mnras/stad664)

van der Walt, S., Schönberger, J. L., Nunez-Iglesias, J., et al. 2014, PeerJ, 2, e453, doi: [10.7717/peerj.453](https://doi.org/10.7717/peerj.453)

Varga, T. N., DeRose, J., Gruen, D., et al. 2019, MNRAS, 489, 2511, doi: [10.1093/mnras/stz2185](https://doi.org/10.1093/mnras/stz2185)

Virtanen, P., Gommers, R., Oliphant, T. E., et al. 2020, Nature Methods, 17, 261, doi: [10.1038/s41592-019-0686-2](https://doi.org/10.1038/s41592-019-0686-2)

Wang, Z., Bovik, A., Sheikh, H., & Simoncelli, E. 2004, IEEE Transactions on Image Processing, 13, 600, doi: [10.1109/TIP.2003.819861](https://doi.org/10.1109/TIP.2003.819861)

APPENDIX

A. API DEMONSTRATION

In what follows we illustrate the BTK API to generate blended images, run a deblender on these, and evaluate the performance of the deblender using detection metrics within BTK. This code example is a condensed version of our “quickstart” tutorial (see Section 4).

```
import btk

# setup CATSIM catalog
catalog_name = "../data/input_catalog.fits"
catalog = btk.catalog.CatsimCatalog.from_file(catalog_name)

# setup survey parameters
survey = btk.survey.get_surveys("LSST")

# setup sampling function
# this function determines how to organize galaxies in catalog into blends
stamp_size = 24.0
sampling_function = btk.sampling_functions.DefaultSampling(
    catalog=catalog, max_number=5, max_mag=25.3, stamp_size=stamp_size
)

# setup generator to create batches of blends
batch_size = 100
draw_generator = btk.draw.blends.CatsimGenerator(
    catalog, sampling_function, survey, batch_size, stamp_size
)

# get batch of blends
blend_batch = next(draw_generator)

# setup deblender (we use SEP in this case)
deblender = btk.deblend.SepSingleBand(
    max_n_sources=5,
    use_band=2 # measure on 'r' band
)

# run deblender on generated blend images (all batches)
deblend_batch = deblender(blend_batch)

# setup matcher
matcher = btk.match.PixelHungarianMatcher(pixel_max_sep=5.0) # maximum separation in pixels for matching

# match true and predicted catalogs
truth_catalogs = blend_batch.catalog_list
pred_catalogs = deblend_batch.catalog_list
matching = matcher(truth_catalogs, pred_catalogs) # object with matching information

# compute detection performance on this batch
recall = btk.metrics.detection.Recall(batch_size)
precision = btk.metrics.detection.Precision(batch_size)
print("Recall: ", recall(matching.tp, matching.t, matching.p))
print("Precision: ", precision(matching.tp, matching.t, matching.p))
```

B. SURVEYCODEX

BTK is made to simulate blending scenes for a variety of galaxy surveys. As such, it relies on a careful bookkeeping of the survey parameters, which are usually found scattered among various papers, websites, or code repositories, sometimes without the unit or a proper reference.

In order to improve the consistency of the simulator and prevent the occurrence of bugs in the blending scenes produced for various surveys, a subgroup of BTK developers decided to develop SURVEYCODEX¹⁵, a tiny Python library with referenced survey parameters from the current main galaxy surveys. Consistency was achieved by associating a unit to each of these parameters through the use of `astropy.units` (Astropy Collaboration et al. 2013, 2018, 2022).

The available surveys in SURVEYCODEX for the 1.0 BTK release are given in Table 2. An example of command-line output from SURVEYCODEX for the LSST survey is given in Appendix B.2.

B.1. Description

The library contains parameters describing the telescope (e.g., `mirror_diameter`), the camera (e.g., `pixel_scale` or `gain`), and the characteristics of each of the filters (e.g., `psf_fwhm`, `effective_wavelength`, etc.). Most values have been sourced from official documents or websites, and some like the filters `effective_wavelength` or the `zeropoint` have been computed through the `speclite`¹⁶ package that references the filter responses of most of these surveys. A description of each parameter it holds, carefully sourced or checked with specialists from each survey, can be found in the online documentation¹⁷.

SURVEYCODEX also incorporates basic utility functions, such as the computation of fluxes in electron counts from a given AB magnitude, or the mean sky level. The former is used within BTK to compute galaxy fluxes from magnitudes in the galaxy catalog and follows the usual convention

$$F = T \cdot 10^{-0.4(m-Z)}, \quad (B1)$$

where F is the flux, T the exposure time, Z the zeropoint, and m the corresponding magnitude.

BTK includes its own Survey class (Section 3.1) that directly inherits and contains the information provided by the SURVEYCODEX library.

SURVEYCODEX v1.1 available entries

Survey name	Telescope	Instrument	Reference
CFHTLS	CFHT	Megacam	Cuillandre & Bertin (2006)
COSMOS	HST	ACS	Koekemoer et al. (2007)
DES	Victor M. Blanco	DECam	Dark Energy Survey Collaboration et al. (2016)
Euclid_VIS	Euclid	VIS	Laureijs et al. (2012)
HSC	Subaru	HSC	Aihara et al. (2018)
LSST	Simonyi	LSST camera	Ivezić et al. (2019)

TABLE 2
SUPPORTED SURVEYS IN SURVEYCODEX AND BTK FOR THE VERSION 1.0 BTK RELEASE.

¹⁵ <https://github.com/LSSTDESC/surveycodex>

¹⁶ <https://github.com/desihub/speclite>

¹⁷ <https://lsstdesc.org/surveycodex/>

B.2. *SURVEYCODEX* command-line example

The following is a reduced example output from the command line utility of the SURVEYCODEX package. This output demonstrates the information accessible within SURVEYCODEX about the LSST survey. After the parameter values, a table is shown with references for each parameter. The number of filters and the reference table at the bottom have been shortened for display purposes in this paper.

```
$ surveycodex -s LSST --ref --rich
                                         LSST
Legacy Survey of Space and Time (LSST)
done with the Simonyi survey telescope
and the LSST camera

Pixel scale:          0.200 arcsec
Mirror diameter:     8.36 m
Effective area:      33.34 m2
Obscuration:         0.39
Gain:                1.00 electron / adu
Zeropoint airmass:   1.2
Available filters:   u, g, r, i, z, y

Filter info:
- u
PSF FWHM:            0.90 arcsec
Zeropoint:            26.40 mag
Sky brightness:       22.99 mag / arcsec2
Full exposure time:  1680 s
Effective wavelength: 368.1 nm

- g
PSF FWHM:            0.86 arcsec
Zeropoint:            28.26 mag
Sky brightness:       22.26 mag / arcsec2
Full exposure time:  2400 s
Effective wavelength: 486.4 nm
```

Parameter	Source	LSST references	Comments
pixel_scale	https://www.lsst.org/about/camera/features		See Technical details.
gain	https://github.com/LSSTDESC/imSim/blob/main/imsim/stamp.py#L416		
mirror_diameter	https://www.lsst.org/about/tel-site/optical_design		
zeropoint_irmass	https://specite.readthedocs.io/en/latest/filters.html#lsst-filters		
sky_brightness	https://arxiv.org/abs/0805.2366		
...	...		(v5) See Table 2, first row ...